

Transport in Graphene superimposed by a moving Electrical Superlattice Potential

Jürgen Dietel¹ and Hagen Kleinert^{1,2}

¹*Institut für Theoretische Physik, Freie Universität Berlin, Arnimallee 14, D-14195 Berlin, Germany*

²*ICRANeT, Piazzale della Repubblica 1, 10 -65122, Pescara, Italy*

(Dated: Received July 3, 2012)

We calculate dc-conductivities of ballistic graphene undulated by a overlying moving unidirectional electrical superlattice (SL) potential whose SL-velocity is smaller than the electron velocity. We obtain no dependence of the conductivity on the velocity along the direction of the superlattice wavevector. In the orthogonal direction however, the dependence is strong on the velocity especially at voltages where a new Dirac point emerges for zero velocity. It is shown that the infinite graphene system can serve as an ideal motion detector at potentials where the first new Dirac point emerges. There the conductivity is zero at vanishing SL velocities and jumps to infinity when the SL starts moving. For finite systems at voltages where the number of new Dirac points is of the order of the ratio of the electron velocity by the SL-velocity, the modifications to the conductivity of a moving SL is at least of similar magnitude as the conductivity of the stagnant SL.

PACS numbers: 72.80.Vp, 73.21.Cd, 73.22.Pr

I. INTRODUCTION

The electrical conductivity in suspended graphene samples show high mobilities where ballistic transport is seen for samples up to the micron length [1–3]. Due to the quasi-relativistic behavior of its electrons, graphene has a density of states proportional to the electronic energy which is zero at the neutrality point. As a consequence, this leads in ballistic graphene to the phenomenon that the conductivity shows a universal finite behavior [4] whose precise value is still under debate [5]. It seems now that the universal conductivity in a wide range graphene sample with highly doped leads has the value $\tilde{\sigma} = 4e^2/\pi h$ [6, 7], where in a system with vanishing small doped leads, it is $\tilde{\sigma} = e^2\pi/2h$ [8]. Numerically, these two values are quite close to each other. A small perturbation of the chemical potential of the graphene sample may be caused by applying an external gate voltage, this conductivity can change drastically, due to the now finite density of states at the Fermi-energy. For an infinite large ballistic system, it becomes even infinite. Such an extreme sensitivity of the neutral graphene system on the environment parameters makes it attractive as a building block for nano-detectors. It was experimentally shown that graphene is a good chemical sensor which is able to detect the dc-response changes due to the adsorption of even single gas molecules on its surface [9]. This high sensitivity is mainly due to the intrinsic low-noise properties of graphene. A more general review of possible graphene sensors can be found in Ref. 10.

Here we consider a ballistic graphene sample with an overlying slowly moving unidirectional electrical SL. We calculate the longitudinal conductivities along and orthogonal to the SL wavevector as a response of a small external dc-field. This system is considered as a possible model for a graphene-based nanomechanical motion detector.

In the direction orthogonal to the wavevector of the SL we obtain, especially at SL voltages where new Dirac

points emerges in the non-moving SL, a high sensitivity of the conductivity values on the SL-motion. In the parallel direction our approximation produces no dependence on the SL-velocity.

Graphene under the effect of a moving SL can be realized for example by placing periodically patterned gate electrodes on either a moving underlying substrate or on a rested substrate where now the individual gate electrodes are activated appropriately with time such that an effective moving SL is simulated. More directly, the experimental realization could be also carried out by using the coupling of the graphene sheet to the electrical field of a surface acoustic wave on a piezoelectric substrate [11] or to a charged moving membrane with ripples.

It was recently shown explicitly for graphene that new Dirac points in the energy spectrum can be opened by imposing a non-moving SL on the graphene lattice [12–14]. This leads to unusual conductivity properties in such systems [15–18]. These new Dirac points are accompanied with new energy valleys. Due to the technical complications in handling transport in a moving SL we will consider at first the transport contributions of the inner-valleys near the \mathbf{K} and \mathbf{K}' points in Sect. III, then those of the outer-valleys in Sect. IV. Note, that such a separation is not useful for the non-moving SL as will be seen in Sect. IV. We start in Sect. II by reconsidering first the lowest-band eigenvalues and eigenfunctions for the non-moving SL.

We discuss here the most simple representation of a SL being a symmetric two-step Kronig-Penney potential with a superlattice potential $V(x) = V\chi(x)$ where $\chi(x) = \text{sg}[\sin(2\pi x/d)]$ (cf. Fig. 1). The function $\text{sg}[x]$ is the sign of x , and d is the wavelength of the SL. In the continuum approximation, the graphene Hamiltonian under consideration near the Dirac point \mathbf{K} is given by $H_{v_s} = \hbar v_F(\sigma_x \partial_x/i + \sigma_y \partial_y/i) + V(x + v_s t)$ [4]. Here v_F is the Fermi velocity and $\sigma_{x,y}$ are the Pauli matrices, while v_s is the velocity of the moving SL.

II. LOWEST BAND EIGENVALUES AND EIGENFUNCTIONS

In the following, we solve the eigenvalue equation $H_{v_s} \mathbf{u}^{v_s}(\mathbf{r}') = \epsilon \mathbf{u}^{v_s}(\mathbf{r}')$ for a non-moving SL ($v_s = 0$) by using the transfer matrix method [16, 19]. For the energy dispersion in the lowest band we restrict ourselves to the lowest-lying oscillatory regime $|\epsilon_s|d/\hbar v_F \ll \tilde{V}, \tilde{\alpha}_0$ and obtain [20]

$$\epsilon_s = s\hbar v_F \tilde{\alpha}_0^2 \sqrt{k_x^2 + |\Gamma|^2 k_y^2}, \quad (1)$$

with $\alpha_{\epsilon_s}(x) = \{[(\epsilon_s - V(x))/\hbar v_F]^2 - k_y^2\}^{1/2} d/2$, $\Gamma = \sin[\alpha_0] e^{i\alpha_0}/\alpha_0$, $\tilde{\alpha}_0 = \alpha_0/\tilde{V}$ where $\tilde{V} = Vd/2\hbar v_F$. The Bloch momentum in x -direction is restricted to $-\pi/d \leq k_x \leq \pi/d$. The parameter $s = 1$ denotes the conduction band and $s = -1$ the valence band.

The corresponding lowest-band eigenfunctions are $\mathbf{u}^{v_s}(x, y) = e^{ik_y y} \mathbf{u}^{v_s}(x)$, in the fundamental zone $0 \leq x \leq d$ and for $v_s = 0$ reduces to $\mathbf{u}_s^0(x) = \Lambda(x) \mathbf{u}_s^0(0)$ with $\Lambda(x) = \lambda_0(x) \Theta(d/2 - x) + \lambda_{d/2}(x) \lambda_0(d/2) \Theta(x - d/2)$, where

$$\lambda_{x_0}(x) = \cos \left[\frac{\alpha_{\epsilon_s}(x) 2(x - x_0)}{d} \right] \mathbf{E} + \frac{\sin \left[\frac{\alpha_{\epsilon_s}(x) 2(x - x_0)}{d} \right]}{\alpha_{\epsilon_s}(x)} \mathbf{M}. \quad (2)$$

Here \mathbf{E} is the unit matrix and $\mathbf{M} = k_y \sigma_3 + i[\epsilon_s - V(x)] \sigma_2 / \hbar v_F$. $\mathbf{u}_s^0(0)$ is given in the oscillatory region $|\epsilon_s|d/\hbar v_F \ll \tilde{V}, \tilde{\alpha}_0$ by

$$\mathbf{u}_s^0(0) \approx \frac{1}{N_u} \begin{pmatrix} \frac{\cos(\alpha_0) \sin(\alpha_0)}{\alpha_0} k_y d + i k_x d \\ i \frac{1}{\alpha_0^2} \frac{\epsilon_s d}{\hbar v_F} + i \frac{\sin^2(\alpha_0)}{\alpha_0^2} \tilde{V} k_y d \end{pmatrix}, \quad (3)$$

where N_u in (3) denotes a normalization factor. From (1) we obtain an oscillatory behavior of the lowest band eigenvalues as a function of k_y (cf. Fig. 1). New Dirac points emerge at $\mathbf{k} = 0$ for $\tilde{V} \in \mathbb{N}\pi$. These are shifted along the y -axis in \mathbf{k} -space for increasing \tilde{V} . Note that the lowest band energy values beyond the oscillatory regime with momenta $k_y^2 \gg (V/\hbar v_F)^2$ scale like $|\epsilon_s| \sim \hbar v_F |k_y|$ [16, 19].

In the following, we discuss the transport contributions of electrons in the inner-energy valleys where $k_y \ll V/\hbar v_F$ and the outer-valleys where $\tilde{\alpha}_0 \ll 1$ separately.

III. INNER-VALLEY TRANSPORT CONTRIBUTIONS

In the inner-valley regime $k_y \ll V/\hbar v_F$, the lowest-band eigenfunctions $\mathbf{u}_s^0(x)$ for the non-moving system stated above are given by

$$\mathbf{u}_s^0(x) = \frac{1}{N_u} \begin{bmatrix} \left(\frac{1}{1} \right) \left(\frac{-ik_x}{k_y \Gamma^*} - \frac{i\epsilon_s}{\hbar v_F k_y \Gamma^*} \right) \phi_+(x) + \begin{pmatrix} -1 \\ 1 \end{pmatrix} \phi_-(x) \end{bmatrix}, \quad (4)$$

where \tilde{N}_u in (4) denotes a normalization factor. The phase factor $\phi_{\pm}(x)$ is given by $\phi_{\pm}(x, t) = \exp[iS_{\pm}^{v_s}(x, t)/\hbar]$ with $S_{\pm}^0(x, t) = \mp i\hbar \int_0^x dx' \text{sgn}[V(x')] \alpha_{\epsilon_s}(x')/(d/2) - i\epsilon_s t$ for $v_s = 0$ chosen such that \mathbf{u}_s^0 solves simultaneously the corresponding time-dependent Schrödinger equation (TSE). From (4) we deduce the remarkable observation that the inner-valley electrons do not backscatter at the potential steps. This phenomenon is well known for ordinary Dirac-fermions as Klein-paradox.

In the following, we use the inner-valley approximation $\alpha_0(x) \approx \tilde{V}(1 - \tilde{k}_y^2/2)$ with $\tilde{k}_y = \hbar v_F q/V$ in (1), (4) that is a good approximation of the overall oscillatory behavior of the energy dispersion in Fig. 1. Similar approximations will also be used when solving the TSE for $v_s \neq 0$ below. Finally we note that the missing of the k_x, k_y dependence in the vector part $(\mp 1, 1)^T$ of both spinor components in (4) is due to the inner-valley restriction $k_y^2 \ll (V/\hbar v_F)^2$.

We obtain from (1) that an entire set of $2[\tilde{V}/\pi] + 1$ Dirac points exists near \mathbf{K} where $[x]$ is the lowest integer number smaller than x . By using the inner-valley approximation discussed above, these new Dirac points are located at $k_y^n d \approx 2[2\tilde{V}(\tilde{V} - \pi n)]^{1/2}$ with $n = 1 \dots [\tilde{V}/\pi]$ and $k_y^0 = 0$ (restricting ourselves to positive k_y). The linearized energy spectrum around these Dirac points is given by $\epsilon_s^n = s\hbar v_F [k_x^2 + \Gamma_n^2 (k_y - k_y^n)^2]^{1/2}$ where the effective y -velocity coefficient is given by $\Gamma_n \approx 2[1 - n\pi/\tilde{V}]$ for $n = 1, \dots, [\tilde{V}/\pi]$, and $\Gamma_0 = \sin(\tilde{V})/\tilde{V}$ for the central valley. The magnitude $\tilde{\alpha}_0$ for $k_y = k_y^n$ is given by $\pi n/\tilde{V}$. Below, we shall also need the k_y -momentum spacings between the right and left-energy crest and the Dirac point. The spacing for the right crest is given by $\Delta k_y^{n,R} d \approx \pi[\tilde{V}/2(\tilde{V} - \pi n)]^{1/2}$ for $n = 1, \dots, [\tilde{V}/\pi]$ and $\Delta k_y^{n,L} = \Delta k_y^{n,R}$ for the left crest positions where $n = 1 \dots [\tilde{V}/\pi] - 1$. For the central crest distance we obtain $\Delta k_y^{0,R} d = \Delta k_y^{0,L} d \approx (k_y^{[\tilde{V}/\pi]} d)^3 / [(k_y^{[\tilde{V}/\pi]} d)^2 + 4\Gamma_0 \tilde{V}^2]$ and $\Delta k_y^{[\tilde{V}/\pi],L} = k_y^{[\tilde{V}/\pi]} - \Delta k_y^{0,L}$. Finally we note that the inner-valley formula with $k_y^2 \ll 1$ considered in this subsection is valid for the valleys $1 - \pi n/\tilde{V} \ll 1$ with $n \neq 0$ and also the central valley $n = 0$.

In the following we solve the TSE $i\hbar \partial_t \mathbf{u}_s^{v_s}(x, t) = H_{v_s} \mathbf{u}_s^{v_s}(x, t)$ with the initial condition $\mathbf{u}_s^{v_s}(x, 0) = \mathbf{u}_s^0(x)$ for $t = 0$ in the oscillatory regime by using the above approximations. Note that by using the characteristic-method we can solve the TSE without approximation for $k_y = 0$. This leads again to (4) where now $S_{\pm}^{v_s}$ is v_s -dependent. Instead of doing this explicitly, we can generalize this procedure to any non-zero $k_y^2 \ll (V/\hbar v_F)^2$ by the Hamilton-Jacobi Ansatz

$$-\frac{\partial S_{\pm}^{v_s}}{\partial t} = -\hbar v_F \text{sgn}[V(x + v_s t)] \sqrt{(\partial_x S_{\pm}^{v_s})^2 + k_y^2} + V(x + v_s t) \quad (5)$$

with the boundary condition that $S_{\pm}^{v_s}(x, 0) = S_{\pm}^0(x, 0)$. Due to the local uniformity of $V(x + v_s t)$ in position and time we obtain local uniform solutions of (5). That this

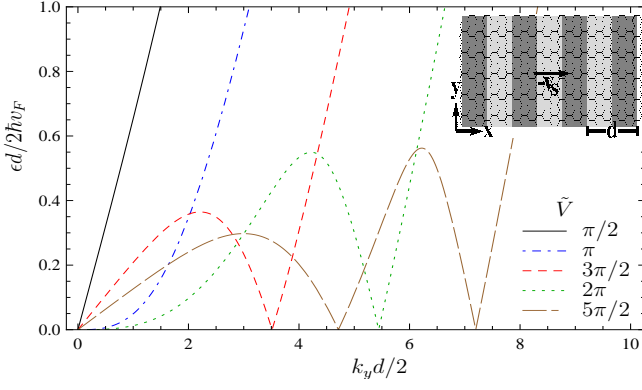


FIG. 1: (Color online) Lowest Bloch band energy spectrum for $k_x = 0$ as a function of dimensionless momenta k_y for various SL potential strengths \tilde{V} (the full lowest band energy spectrum can be obtained by using its mirror symmetry with respect to the x,y-axis). Here we used the transfer matrix method [16, 19]. Inset shows a graphene layer with an overlying moving SL in x-direction.

approach leads to a TSE solution in the oscillatory regime is due to the fact that the general solution can be written as

$$\mathbf{u}_s^{v_s}(x, t) \approx \sum_{s, k_x} a_{s, k_x} \begin{pmatrix} s \frac{k_x}{|k_x|} \\ 1 \end{pmatrix} e^{-\frac{i}{\hbar} t [\hbar v_F s \sqrt{k_x^2 + k_y^2} + V(x + v_s t)]} e^{i k_x x} \quad (6)$$

in the inner-valley regime $k_y^2 \ll k_x^2$. The complex variables a_{s, k_x} are local uniform functions in the (x, t) -plane. We will show below that a_{s, k_x} is non-zero for only two special k_x -values which moreover fulfil the inner-valley regime condition $k_y^2 \ll k_x^2$.

We now solve (5) by using a generalized characteristic method for the Hamilton-Jacobi equation that is well known in the semi-classical approach to quantum mechanics [21]. This is based on the one-particle mechanical trajectory of a relativistic particle and anti-particle in a step-potential. The calculation is outlined in App. A.

After some manipulation we obtain the result $S_{\pm}^{v_s}(x, t) \approx S_{\pm}^{v_s, x} + S_{\pm}^{v_s, t}$ with $S_{\pm}^{v_s, t} = -t\epsilon_s$, $Z_{\pm} = v_s^3(v_s \pm v_F)/(v_s^2 - v_F^2)^2$, and

$$S_{\pm}^{v_s, x} = \pm [A_{\pm} \xi(x^* + v_s^* t) + B_{\pm} \xi(x^* \mp v_F^* t) + C_{\pm} t \chi(x^* \mp v_F^* t)], \quad (7)$$

where $\xi(x) = \int_0^x dx' \chi(x')$, $x^* = x - (v_s^* - v_s)t$ and

$$\begin{aligned} A_{\pm} &= \mp \frac{V}{v_s \pm v_F} \left[1 - \tilde{k}_y^2 \frac{v_s \pm \frac{1}{2} v_F}{v_s \pm v_F} + \tilde{k}_y^2 Z_{\pm} \right], C_{\pm} = \pm V \tilde{k}_y^2 Z_{\pm}, \\ B_{\pm} &= -\frac{V}{(v_s \pm v_F)} \left[\frac{v_s}{v_F} - \frac{\tilde{k}_y^2 v_s}{2 v_F} \frac{v_s}{v_s \pm v_F} \mp \tilde{k}_y^2 Z_{\pm} \right], \\ v_F^* &= v_F \left[1 - \frac{\tilde{k}_y^2 (v_s^2 + v_F^2)^2}{2 (v_s^2 - v_F^2)^2} \right], v_s^* = v_s \left[1 - \tilde{k}_y^2 \frac{v_F^2 (v_s^2 + v_F^2)}{(v_s^2 - v_F^2)^2} \right]. \end{aligned} \quad (8)$$

We restrict here the solution of (5) to small velocities $v_s \lesssim v_F$.

Next we calculate the dc-response in the moving SL system. This is done in the gauge $\mathbf{A} = -c\mathbf{E}(t - t_0)\Theta(t - t_0)$ assuming $t_0 \leq 0$ in general. Since $\tilde{\sigma}_{ii}(t)$ does not depend on t_0 for $t \gg 0$ we set immediately $t_0 = 0$. The total Hamiltonian in the continuum approximation is then given by $H_A = H_{v_s} + \hbar v_F (e/c)(\sigma_x A_x + \sigma_y A_y)$. The corresponding TSE-solution which we expand to first order in \mathbf{A} and assume it to satisfy the initial condition $\mathbf{u}_A(t = 0) = \mathbf{u}_s^0$ is denoted by \mathbf{u}_A . From this solution we obtain the conductivity in the i -th direction by $\tilde{\sigma}_{ii} = \lim_{E_i \rightarrow 0} e v_F (\langle \mathbf{u}_A(t) \sigma_i \mathbf{u}_A(t) \rangle / E)$ where $\mathbf{A} = -cE\mathbf{e}_i t$. Here \mathbf{e}_i is the unit vector in the i -th direction. The conductivity in the i -th direction in the lowest energy level approximation valid for $t \rightarrow \infty$ and $v_s \lesssim v_F$, Vd/\hbar is then given by [8]

$$\tilde{\sigma}_{ii}(t) = \frac{-4ev_F}{(2\pi)^2} \int_{\text{BZ}} d^2 k \text{Re}[\langle \mathbf{u}_{-1}^{v_s}(t) | \sigma_i | \mathbf{u}_{+1}^{v_s}(t) \rangle \xi_+(t)] \quad (9)$$

with

$$\begin{aligned} \xi_+(t) &= i \frac{ev_F}{\hbar} \int_0^t dt' t' \mathcal{T}^{v_s}(t') \\ &= i \frac{ev_F}{\hbar} \left(t \int_{t'=-\infty}^t dt'' - \int_{t'=0}^t dt' \int_{t''=-\infty}^{t'} dt'' \right) \mathcal{T}^{v_s}(t'') \end{aligned} \quad (10)$$

and the transition matrix element $\mathcal{T}^{v_s}(t) = \langle \mathbf{u}_1^{v_s}(t) | \sigma_i | \mathbf{u}_{-1}^{v_s}(t) \rangle$. By inserting (10) in (9) the term proportional to t cancels in an improved tight-binding approximation since it can be written as $t \int_{\text{BZ}} d^2 k \partial_{k_i} \langle \mathbf{u}_{-1}^{v_s}(t) | J_i | \mathbf{u}_{-1}^{v_s}(t) \rangle = 0$, where J_i is the tight-binding current operator for $\mathbf{A} = 0$ [8]. Here we used the fact that the exact tight-binding wave functions are smooth at the Brillouin zone boundary. Summing the Fourier series $\sum_{\omega_n} \hat{\mathcal{T}}_r^{v_s}(\omega_n) e^{i\omega_n t} \equiv e^{-it\Delta\epsilon/\hbar} \mathcal{T}^{v_s}(t)$ where $\Delta\epsilon = \epsilon_1 - \epsilon_{-1}$ we obtain for large times

$$\begin{aligned} \xi_+(t) &= i \frac{ev_F}{\hbar} \sum_{\omega_n} \left\{ \frac{\hat{\mathcal{T}}_r^{v_s}(\omega_n)}{(\omega_n + \Delta\epsilon/\hbar - i\delta)^2} \left(e^{i(\frac{\Delta\epsilon}{\hbar} + \omega_n)t} - 1 \right) \right. \\ &\quad \left. - it \frac{[\hat{\mathcal{T}}_r^{v_s}(\omega_n) - \hat{\mathcal{T}}_r^0(\omega_n)]}{\omega_n + \Delta\epsilon/\hbar - i\delta} \right\}. \end{aligned} \quad (11)$$

In the following we calculate the contribution of every energy valley to the momentum integral in (9) separately, i.e. $\tilde{\sigma}_{ii}(t) = \sum_{n=0..[\tilde{V}/\pi]} \tilde{\sigma}_{ii}^n(t) (2 - \delta_{n,0})$. For large times one can restrict the k_y -integrals of Eq. (9) to the neighbourhood of the valley center k_y^n setting immediately $k_y \approx k_y^n$ in $\hat{\mathcal{T}}_r^{v_s}$. Then we obtain by partial integration

$$\begin{aligned} &\int_{n\text{-th valley}} d^2 k \frac{(2\hbar v_F k_x)^2}{(\Delta\epsilon)^2} e^{-\frac{i}{\hbar} \Delta\epsilon t} \xi_+(t) \\ &= \frac{ie}{2\hbar} \frac{1}{\Gamma_n} \left\{ \int_{-\infty}^{+\infty} dk_x \int_{\Delta k_y^n, L \Gamma_n}^{\Delta k_y^n, R \Gamma_n} dk_y \frac{k_x^2}{k^3} F^{v_s}(k) \right. \\ &\quad \left. - \int_0^{2\pi} d\vartheta k_{\vartheta} \sin^2(\vartheta) [F^{v_s}(k_{\vartheta}) - F^0(k_{\vartheta})] \right\} \end{aligned} \quad (12)$$

with

$$F^{v_s}(k) = \frac{\hat{T}_r^{v_s}(\omega_n) e^{i\omega_n t}}{\omega_n + 2v_F k - i\delta} (1 - e^{-i(2v_F k + \omega_n)t}) \quad (13)$$

and $k_\vartheta = (\tan^2(\vartheta) + 1)^{1/2} \Gamma_n \{ \Delta k_y^{n,R} \Theta[\cos(\vartheta)] + \Delta k_y^{n,L} \Theta[-\cos(\vartheta)] \}$ where $\Theta(x)$ is the Heaviside function.

In the calculation of $\tilde{\sigma}_{ii}$ via (9), the quantities $\mathcal{P} \equiv \int_0^d dx \exp^{i(S_+ - S_-)}/d$ and further $\mathcal{C}_m \equiv \sum_{\omega_n \approx 2m\pi v_F^*/d} |\hat{\mathcal{P}}|(\omega_n) (2 - \delta_{n,0}) e^{i\omega_n t}$ are relevant where $|\hat{\mathcal{P}}|(\omega_n)$ are the Fourier components of $|\mathcal{P}|(t)$. More precisely, \mathcal{C}_m with $m > 0$ are the positive components for frequencies $2\pi(m - 1/2)v_F^*/d \leq \omega_n \leq 2\pi(m + 1/2)v_F^*/d$ under the restriction that $\omega_n \geq 0$ for $m = 0$. A straightforward calculation leads with (7) for $v_s \lesssim v_F$ to

$$\begin{aligned} \text{Re}[\mathcal{C}_m] &= \sum_{\sigma \in \{\pm\}} \cos(C_- t) B_- X(m, m, m, \sigma) \\ &\quad - \sin(C_- t) \left[\sigma \frac{2\pi m}{d} + \xi(2v_s^* t) B_+ \right] X(m, m, m + 1, \sigma) + \text{Ex}, \\ \text{Im}[\mathcal{C}_m] &= \sum_{\sigma \in \{\pm\}} \sigma \cos(C_- t) B_- X(m, m, m + 1, \sigma) \\ &\quad + \sigma \sin(C_- t) \left[\sigma \frac{2\pi m}{d} + \xi(2v_s^* t) B_+ \right] X(m, m, m, \sigma) + \text{Ex} \end{aligned} \quad (14)$$

where

$$\begin{aligned} X(n_\omega, n_1, n_2, \sigma) &\approx -\frac{1}{Ad^2} \frac{8(2 - \delta_{n_\omega, 0})}{B_-^2 - [\xi(2v_s^* t) B_+ + \sigma \frac{2\pi n_\omega}{d}]^2} \\ &\quad \sin \left[A \frac{d}{4} + n_1 \frac{\pi}{2} \right] \sin \left[-B \frac{d}{4} + B_+ \xi(2v_s^* t) - C_+ t \chi(2v_s^* t) \right. \\ &\quad \left. - \sigma n_\omega \frac{2\pi v_F^* t}{d} \left(1 - \frac{v_s^*}{v_F^*} \right) + n_2 \frac{\pi}{2} \right]. \end{aligned} \quad (15)$$

The term Ex in (14) stands for the foregoing expressions with interchanged $B_+ \Leftrightarrow B_-$, $C_+ \Leftrightarrow -C_-$ and switched sign of v_s^* . We used further the abbreviation $A \equiv A_+ + A_-$, $B \equiv B_+ + B_-$.

We are now able to calculate the conductivity contribution $\tilde{\sigma}_{ii}^n$ of the n -th energy valley by using (9), (12), (14), leading to

$$\begin{aligned} \tilde{\sigma}_{xx}^n &\approx \frac{e^2}{h} \tilde{\alpha}_0^2 \frac{\pi}{2\Gamma_n}, \\ \tilde{\sigma}_{yy}^n &\approx \frac{e^2}{h} \frac{1}{\tilde{\alpha}_0^2} \frac{\pi}{2\Gamma_n} \sum_{\sigma \in \{L, R\}} \text{Re}[\mathcal{C}_0 + \mathcal{C}_1] \left\{ \text{Re}[\mathcal{C}_0] \right. \\ &\quad \left. + \text{Re}[\mathcal{C}_1] \left[\frac{1}{\pi} \left\{ \vartheta_\sigma^n - \frac{1}{2} \sin(2\vartheta_\sigma^n) \right\} - I_1 \left(\frac{\Gamma_n \Delta k_y^{n,\sigma} d}{\pi}, \vartheta_\sigma^n \right) \right] \right. \\ &\quad \left. - \text{Im}[\mathcal{C}_1] \left[I_2 \left(\frac{\Gamma_n \Delta k_y^{n,\sigma} d}{\pi} \right) + I_3 \left(\frac{\Gamma_n \Delta k_y^{n,\sigma} d}{\pi} \right) \right] \right\}. \end{aligned} \quad (16)$$

Terms containing \mathcal{C}_m with $m \geq 2$ are neglected here which can be justified numerically. The angle ϑ_σ^n is given by $\tan(\vartheta_\sigma^n) = (\Gamma_n d \Delta k_y^{n,\sigma}) / [\pi^2 - (\Gamma_n d \Delta k_y^{n,\sigma})^2]^{1/2}$. The

functions I_1, \dots, I_3 are calculated from (12) for $t \rightarrow \infty$ as

$$\begin{aligned} I_1(x, \varphi) &= \frac{2}{\pi x^2} \sin^3(\varphi) |\cos(\varphi)|, \\ I_2(x) &= \frac{2}{\pi^2} x + \frac{2}{\pi^2} \text{sgn}[1 - x^2] \text{Re} \left\{ \frac{a(x)}{4} \left[\csc^2 \left(\frac{a(x)}{2} \right) \right. \right. \\ &\quad \left. \left. - \sec^2 \left(\frac{a(x)}{2} \right) \right] - \sum_{\sigma \in \{\pm\}} \sigma \left[a(x) \log(1 + \sigma e^{ia(x)}) + i \text{Li}_2(\sigma e^{ia(x)}) \right] \right\}, \\ I_3(x) &= \frac{4}{\pi^2} x \left(\sqrt{x^2 - 1} a(x) - 1 \right), \end{aligned} \quad (17)$$

where $a(x) \equiv \arctan(1/\sqrt{x^2 - 1})$. We obtain from (16) that the conductivity $\tilde{\sigma}_{xx}^n$ does not depend on v_s , whereas $\tilde{\sigma}_{yy}^n$ shows a strong v_s -dependence. For $v_s = 0$, $\tilde{\sigma}_{yy}^n$ is reduced to $\tilde{\sigma}_{yy}^n = \delta_{n,0} \Gamma_n e^2 \pi / 2h$. Furthermore we find for $\tilde{\sigma}_{xx}^0$ a divergence at SL potentials where $\tilde{V} \in \mathbb{N}\pi$ for general velocities. The same thing holds for $\tilde{\sigma}_{yy}^0$ but here we must demand $v_s > 0$. The origin of these divergences comes from the vanishing of Γ_0 . All this and the result of the next section leads us to the remarkable fact that an infinite large SL graphene sample is an *ideal motion detector* at SL potentials where the first new Dirac point emerges, i.e. at $\tilde{V} = \pi$: There $\tilde{\sigma}_{yy}$ is vanishing for $v_s = 0$ and jumps to infinity for $v_s \neq 0$.

From (11), (12), the divergence of $\tilde{\sigma}_{yy}^0$ at $\tilde{V} \in \mathbb{N}\pi$ has its origin in the approximation that we used an infinite ballistic time $t \sim t_b$ in calculating the response. This is not really valid for a finite system where $t_b \sim L/v_f$ and L is the length of the sample. By repeating the discussion below (10) but use the energy $\epsilon_s \approx \hbar v_F (k_x^2 + d^4 k_y^6 / 64 \tilde{V}^4)^{1/2}$ at $\tilde{V} \in \mathbb{N}\pi$ leads to $\tilde{\sigma}_{ii}^0$ in (16) with a finite cut-off at $1/\Gamma_0 \sim (\tilde{V} t_b)^{2/3}$. In the following we calculate from (11) the conductivities σ_{ii}^0 at $\tilde{V} \in \mathbb{N}\pi$ in leading order in $1/t_b$ for $t_b \rightarrow \infty$. The results are $\tilde{\sigma}_{ii} \approx \tilde{\sigma}_{ii}^0$ with

$$\begin{aligned} \tilde{\sigma}_{xx}^0 &= \frac{e^2}{h} \frac{\sqrt{3}}{4^{2/3} \sqrt{\pi}} \frac{\Gamma(1/6) \Gamma(1/3)}{\Gamma(2/3)} \left(\tilde{V} \frac{v_F t_b}{d} \right)^{2/3}, \\ \tilde{\sigma}_{yy}^0 &= \frac{e^2}{h} \frac{\sqrt{3}}{4^{2/3} \sqrt{\pi}} \frac{\Gamma(1/6) \Gamma(1/3)}{\Gamma(2/3)} \left(\tilde{V} \frac{v_F t_b}{d} \right)^{2/3} \text{Re}[\mathcal{C}_0 + \mathcal{C}_1] \text{Re}[\mathcal{C}_{00}] \end{aligned} \quad (18)$$

where $\mathcal{C}_{00} = (v_s/d) \int_0^{d/v_s} dt \mathcal{C}_0$. By using (14) we obtain

$$\text{Re}[\mathcal{C}_{00}] = \frac{32 \sin(A \frac{d}{4})}{B_+ B_- A d^3} \left[\cos \left(\left\{ B_+ - B_- \right\} \frac{d}{4} \right) - \cos \left(B \frac{d}{4} \right) \right]. \quad (19)$$

In Fig. 2 we plot $\tilde{\sigma}_{yy}$ for $v_s/v_F = 0.1$ (left panel) and $v_s/v_F = 0.01$ (right panel), as well as for $v_s = 0$ (horizontal curves) at various \tilde{V} -values. The most interesting \tilde{V} -values are where for a certain v_s the signal $\tilde{\sigma}_{yy}$ is largest. In particular, the signal to background ratio, i.e., $\tilde{\sigma}_{yy}$ divided by $\tilde{\sigma}_{yy}$ for $v_s = 0$, should be large. We obtain from the figure and (16) as well as (18) that for a finite system and $v_s \ll v_F$, the SL potential region where $\tilde{V} \sim v_F/v_s$ and $\tilde{V} \in \mathbb{N}\pi$ gives the best results. We plot this in Fig. 2

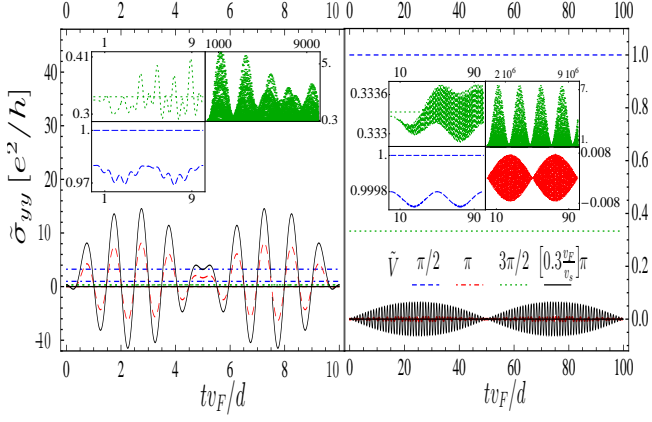


FIG. 2: (Color online) We show the conductivity $\tilde{\sigma}_{yy}$ orthogonal to the SL calculated for velocities $v_s/v_F = 0.1$ (left panel) and $v_s/v_F = 0.01$ (right panel) as a function of the dimensionless time. We plot the curves for various SL-potentials \tilde{V} by using (16) for $\tilde{V} \notin \mathbb{N}\pi$, (18) for $\tilde{V} \in \mathbb{N}\pi$ and ballistic times $(v_F t_b/d)^{2/3} = 1000$. The horizontal curves show $\tilde{\sigma}_{yy}$ for $v_s = 0$. Insets in both panels show a zoom in of the corresponding curves in the main panels where we add for $\tilde{V} = 3\pi/2$ an inset showing $\tilde{\sigma}_{yy}$ also for larger times.

for $\tilde{V} = [0.3v_F/v_s]\pi$. This is chosen so that the curves do not show a higher-order v_s -Fourier behavior according to (14). We note that in principle a graphene velocity detector based on a SL considered here could also attain a large signal to background conductivity for small velocity differences by using large SL potentials $\tilde{V} \sim v_F/\Delta v_s$. This is due to the phase factors in (14).

Beside the oscillation frequencies $\sim 2\pi v_F^*/d$ and $\sim 2\pi v_s^*/d$ we also find from (14) and Fig. 2 a much smaller oscillation frequency $\sim C_{\pm}$ for the conductivity contribution of the side-valleys becoming relevant only on very large time scales. One can show that due to its non-zero velocity, the SL transfer additional energy and momentum to an electron passing its potential steps such that the electron velocity oscillates between $\pm v_F(1 - \tilde{k}_y^2/2)$ and $\pm v_F[1 - \tilde{k}_y^2(v_F \pm v_s)^2/2(v_F \mp v_s)^2]$. Due to this velocity difference the electron picks up an additional oscillating phase proportional to t represented by the last term in (7). This leads to the long wave-conductivity oscillations shown in Fig. 2.

To complete our discussion, we finally calculate the quasi-particle velocities in the x and y -direction for electrons in the $\mathbf{u}_{\pm 1}^{v_s}$ state where now $E_{dc} = 0$. The knowledge of these velocities is useful in quantum pumping experiments [22, 23]. We obtain from (1) and (4)

$$v_x = v_F \langle \mathbf{u}_{\pm 1}^{v_s} | \sigma_{xx} | \mathbf{u}_{\pm 1}^{v_s} \rangle = \frac{\partial \epsilon_{\pm}}{\hbar \partial k_x}, \quad (20)$$

$$v_y = v_F \langle \mathbf{u}_{\pm 1}^{v_s} | \sigma_{yy} | \mathbf{u}_{\pm 1}^{v_s} \rangle = \frac{\partial \epsilon_{\pm}}{\hbar \partial k_y} |\mathcal{P}| \approx \frac{\partial \epsilon_{\pm}}{\hbar \partial k_y} \text{Re}[\mathcal{C}_0 + \mathcal{C}_1].$$

This means that similar to the above conductivity considerations we obtain no time dependence of v_x , in con-

trast to v_y . As in the non-moving system [24] there is a collimation of the electron motion in x -direction, i.e., $|v_y| \ll |v_x|$ for potentials were $\tilde{V} \approx \mathbb{N}\pi$ and momenta k_y near the central Dirac point. Here we use that $|\mathcal{P}| \leq 1$.

IV. OUTER-VALLEY TRANSPORT CONTRIBUTIONS

Next, we discuss the conductivity contributions of the outer-energy valleys where $\tilde{\alpha}_0 \ll 1$. We obtain from (1) that the new Dirac points are located at $k_y^n d/2 = [\tilde{V}^2 - (\pi n)^2]^{1/2}$ where the linearized energy spectrum around these points is given by $\epsilon_s = s\hbar v_F [\tilde{\alpha}_0^4 k_x^2 + \Gamma_n^2 (k_y - k_y^n)^2]^{1/2}$. The effective y -velocity coefficient is now given by $\Gamma_n = [\tilde{V}^2 - (\pi n)^2]/\tilde{V}^2$ and $\tilde{\alpha}_0 = \pi n/\tilde{V}$. This means that the outer-valley regime $\tilde{\alpha}_0 \ll 1$ is fulfilled for those valleys where $\pi n/\tilde{V} \ll 1$.

We obtain now from Sect. II for the space evolution operator (2) of the non-moving system $\lambda_{x_0}(x) \approx \mathbf{M} \sin(\alpha_{\epsilon_s}(x)2(x - x_0)/d)/\alpha_{\epsilon_s}(x)$ to leading order in $\tilde{\alpha}_0$. The corresponding lowest-band eigenfunctions \mathbf{u}_s^0 can be interpreted by electrons which are fully backscattered close to the potential steps for $|\epsilon_s|d/\hbar v_F \ll \tilde{\alpha}_0$. This is just the opposite situation of the inner-valley transport contributions discussed in Sect. III where we got a complete transmission through the potential steps. This interpretation is even justified by discussing the scattering of electrons on a single potential step in the momentum regime $\tilde{\alpha}_0 \ll 1$. In this regime $\mathbf{u}_s^{v_s}$ can now be written as in (6) with the substitution of the spinor part $(sk_x/|k_x|, 1) \rightarrow (-isk_y/|k_y|, 1)$. For the moving lattice we concentrate us in the following on a particle moving in a potential $\pm V$ in the region $-v_s t \leq x \leq d/2 - v_s t$. We now determine a complete set of functions fulfilling the quasi-relativistic Klein-Gordon equation with a potential $V(x) = \pm V$ obeying the zero-boundary conditions $v^j(-v_s t, t) = v^j(-v_s t + d^*/2, t) = 0$. The distance d^* has a small modification to the distance d for $|\epsilon_s|d/\hbar v_F \ll \tilde{\alpha}_0$ determined by $\alpha_{\epsilon_s} d^*/d = \pi n$ for the n -th energy valley, i.e. $\alpha_0 = \pi n$. These wavefunctions consist of a superposition of two Klein-Gordon wave-function solutions. The momenta of both Klein-Gordon wave-functions can be formally derived from the zero-boundary conditions. More concrete the two corresponding momenta are given by a particle initial momentum and its reflected momentum at the boundary. In the quasi-nonrelativistic limit valid for $v_F |k_x^j/k_y|, |v_s| \ll v_F$ we obtain for these momenta $k_x^j \pm v_s |k_y|/v_F$ and $-k_x^j \pm v_s |k_y|/v_F$ with $j \in \mathbb{N}$ and $k_x^j = 2\pi j/d^*$ in the potential $V(x) = \pm V$. The restriction on the quasi-nonrelativistic limit is justified for the outer-valley transport contributions in the case $v_s \ll v_F$. This leads to

$$v_{\pm}^j(x, t) = \frac{2}{\sqrt{d^*}} e^{\pm i(\hbar v_F \sqrt{k_x^j + k_y^2} - V)t/\hbar} e^{\mp i(1/2)(v_s^2/v_F)|k_y|t} \times e^{\pm i(v_s |k_y|/v_F)(x + v_s t)} \sin[k_x^j(x + v_s t)]. \quad (21)$$

By using (2) and (3), the wavefunction $\mathbf{u}_s^{v_s}$ is then given by

$$\begin{aligned} \mathbf{u}_s^{v_s}(x, t) = & -i \frac{d}{2\alpha_0} \left\{ \text{sg}[k_y V(x + v_s t)] \frac{\cos(\alpha_0) \sin(\alpha_0)}{\alpha_0} k_y^2 d \right. \\ & \left. + 2 \text{sg}[k_y] \frac{\epsilon_s \tilde{V}}{\tilde{\alpha}_0^2} + i \text{sg}[V(x + v_s t)] |k_y| k_x d \right\} \\ & \times \left(\frac{\text{sg}[k_y V(x + v_s t)] i}{1} \right) \sum_j c_j^{\text{sg}[V(x + v_s t)]} v_{\text{sg}[V(x + v_s t)]}^j(x, t) \end{aligned} \quad (22)$$

with

$$c_j^{\text{sg}[V(x + v_s t)]} = \int_0^{d^*/2} dx (v_{\text{sg}[V(x + v_s t)]}^j)^*(x, 0) \sin\left(\alpha_{\epsilon_s} \frac{2x}{d}\right). \quad (23)$$

With this wavefunction in hand we are now prepared to calculate the conductivities $\tilde{\sigma}_{ii}^n$ for the outer-valleys $\pi n / \tilde{V} \ll 1$. By using (9) with (11) and (22) we obtain for the conductivities

$$\tilde{\sigma}_{xx}^n \approx 0 \quad , \quad \tilde{\sigma}_{yy}^n \approx \frac{e^2}{h} \frac{\pi}{2} \frac{1}{\tilde{\alpha}_0^2} |\Gamma_n| Y(v_s) \quad (24)$$

with $Y(v_s)$ is given by

$$Y(v_s) = \sum_{i,j>0} \frac{n^2}{i^2} |c_i|^2 |c_j|^2 (\delta_{i,j} + 2\delta_{i>j}). \quad (25)$$

Here we use $|c_i| = |c_i^\pm|$ and c_i, c_j in (25) and (23) are calculated with $d^* \rightarrow d$.

We obtain from (24) that the transport contributions of the outer-valleys corresponding to $\tilde{\alpha}_0 \ll 1$ show no time-fluctuations. This is not based on the quasi-nonrelativistic approximation used above. We show in Fig. 3 $\tilde{\sigma}_{yy}^n$ for the outer-valleys and various SL potentials \tilde{V} and velocity fractions v_s/v_F . Most pronounced, the curves on the right panel show a conductivity peak at valley indices where $n \approx n_0$. Here n_0 is given by $n_0 = \lceil |v_s/v_F| (\tilde{V}^2 - (\pi n)^2)^{1/2} / \pi \rceil$. This conductivity peak is also observed from (24) and (25) by taking into account that in a rough approximation we have $|c_i|^2 \approx (\delta_{i,n+n_0} + \delta_{i,|n-n_0|})/2$ leading to

$$Y(v_s) \approx \frac{1}{4} \frac{n^2}{|n - n_0|^2} + \frac{3}{4} \frac{n^2}{|n + n_0|^2}. \quad (26)$$

All this means that for $\tilde{V} \gtrsim \pi v_F / v_s$ with $\tilde{V} \gg 1$ we obtain a large conductivity signal where the conductivity modification due to the motion of the SL is of similar magnitude as the conductivity value of the non-moving SL. Similar is of course true for the detection of small velocity differences Δv_s where now we have $\tilde{V} \gtrsim \pi v_F / \Delta v_s$ in order to obtain a large signal to background value. By comparing the conductivity values $\tilde{\sigma}_{yy}^n$ for the inner-valleys (16), Fig. 2 and the outer-valleys (24), Fig. 3 we obtain at least for $\tilde{V} \gg 1$ and $\tilde{V} \not\approx N\pi$ that the outer-valley contributions are dominant.

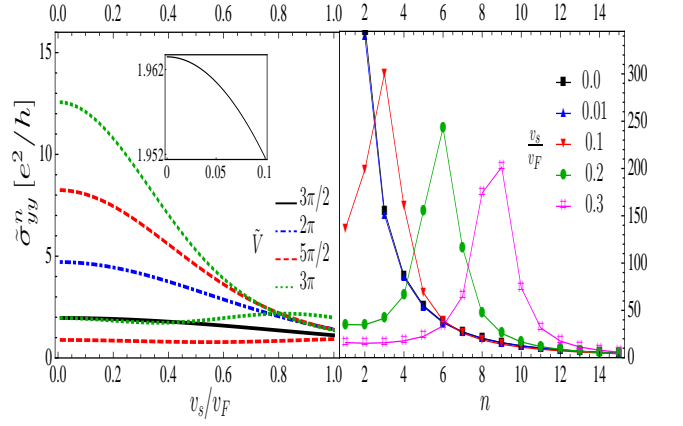


FIG. 3: (Color online) Left panel: Outer valley-conductivities $\tilde{\sigma}_{yy}^n$ (24) of the n -th electron side-valley as a function of v_s/v_F for certain SL potentials. For $\tilde{V} = 5\pi/2$ and $\tilde{V} = 3\pi$, which both consists of two side-valleys, the upper curve corresponds to the valley index $n = 1$ and the lower curve to $n = 2$. Inset shows a zoom in of $\tilde{\sigma}_{yy}^1$ for $\tilde{V} = 3\pi/2$. Right panel: $\tilde{\sigma}_{yy}^n$ for $\tilde{V} = 30\pi$ as a function of the valley index n for certain SL velocities v_s/v_F .

Next, we calculate the effective particle velocities for electrons in the outer-valley defined in (20), where now again $E_{dc} = 0$. By using (21) and (22) we obtain

$$v_x = \frac{\partial \epsilon_{\pm}}{\hbar \partial k_x} \quad , \quad v_y = \frac{\partial \epsilon_{\pm}}{\hbar \partial k_y}. \quad (27)$$

This shows that there is no v_s -correction term in contrast to the inner-valley case (20) for v_y . This is caused by the fact that in the outer-valley regime electrons are approximately fully reflected, and thus the total probability of finding an electron between $-v_s t$ and $-v_s t + d/2$ is conserved.

The non-trivial dependence of the conductivities on the SL-velocity forced us to treat the conductivity contributions for the inner and outer-valleys separately. This separation is no longer necessary when calculating the conductivities for the non-moving SL. For this we use the full oscillatory wave-function (3) with (2) and (9), (11). This leads us to the following $v_s = 0$ -conductivities

$$\tilde{\sigma}_{xx}^n = \frac{e^2}{h} \frac{\pi}{2} \tilde{\alpha}_0^2 \frac{1}{|\Gamma_n|} \quad , \quad \tilde{\sigma}_{yy}^n = \frac{e^2}{h} \frac{\pi}{2} \frac{1}{\tilde{\alpha}_0^2} |\Gamma_n|. \quad (28)$$

Note here that the magnitudes of $\tilde{\alpha}_0$ and Γ_n correspond to the outer-valley values discussed above Eq. (21) for $n \neq 0$ and to the $n = 0$ values discussed above Eq. (5). Similar expressions as in (28) were calculated before within the dc vector potential gauge $\mathbf{A} = 0$, leading as in pristine graphene to a small overall numerical prefactor correction to our result (28) [18]. The disadvantage of the calculation in Ref. 18 lies in the strong dependence of this prefactor on the order of taking the zero-temperature, zero-frequency, and zero-damping limit. This does not happen in our calculation [8].

V. SUMMARY

Summarizing, we have considered the dc-transport in neutral graphene undulated by a unidirectional moving superlattice potential with $v_s \lesssim v_F, Vd/\hbar$. While the response along the direction of the SL wave-vector is vanishing, the dependence is dramatic in the orthogonal direction. In particular we find for potentials where the first new Dirac point emerges, i.e., at $\tilde{V} = \pi$, that the infinite large graphene sample is a perfect motion detector. The orthogonal dc-conductivity is vanishing for zero velocity and jumps to infinity at non-zero SL-velocity. A large conductivity signal with a high signal to background ratio is reached for the finite but large graphene system when $\tilde{V} \in \mathbb{N}\pi$. The time fluctuating contribution to the conductivity is largest when $\tilde{V} \sim v_F/v_s$. All this was derived from the inner-valley contributions to the conductivities.

Next we have calculated the conductivity contributions of the outer-valleys. The conductivity contributions parallel to the SL-wavevector are vanishing. In the orthogonal direction they are large, time-independent and exhibit a peak as a function of the valley index. For $\tilde{V} \gg 1$ and $\tilde{V} \gtrsim \pi v_F/v_s$ the conductivity modifications due to a moving SL are of similar magnitude as the conductivity values of the stagnant SL. Note that for $\tilde{V} \gg 1$ the outer-valley conductivity contributions are dominate over the inner-valley contributions, at least for $\tilde{V} \not\approx \mathbb{N}\pi$. Finally, we have calculated the conductivities of the non-moving SL without the need of a separate calculation for the inner and outer-valleys.

Due to its intrinsic low-noise level [9], our results could be useful for graphene as a nanophysical motion detector

device, or even for general sensors based on the surface acoustic wave technology [25].

Appendix A: Solving the Hamilton-Jacobi equation Eq. (5)

Here we outline the calculation of (7) by solving the Hamilton-Jacobi equation (5) to first order in \tilde{k}_y^2 . This is done with the help of a generalized characteristic method [21]. The solution is based on the one-particle quasi-relativistic orbit $x(t)$ in a moving potential $V(x + v_s t)$. With the help of this solution, $S_{\pm}^{v_s}(x, t)$ is given by the action integral

$$S_{\pm}^{v_s}(x, t) = \int_0^t dt' \left\{ \frac{v_F \hbar^2 k_y^2}{\sqrt{p_t^2(t') + \hbar^2 k_y^2}} \text{sg}[V(x_t(t') + v_s t')] - V(x_t(t') + v_s t') \right\} + S_{\pm}^0(x_0, 0). \quad (\text{A1})$$

Here $x_t(t')$ is the particle trajectory with $x_t(0) = x_0$, $x_t(t) = x$. The particle-momentum is given by $p_{t'}(t) = \partial_x S_{\pm}^{v_s}(x_t(t), t)$ and the quasi-relativistic velocity by

$$\dot{x}_t(t') = -v_F \text{sg}[V(x_t(t') + v_s t')] \frac{p_t(t')}{\sqrt{p_t^2(t') + \hbar^2 k_y^2}}. \quad (\text{A2})$$

We note now that it is much easier to determine $x_t(t')$ by solving the set of equations above for small \tilde{k}_y , instead of solving the second-order quasi-relativistic Newton equation. From this we obtain (7).

-
- [1] S. V. Morozov, K. S. Novoselov, M. I. Katsnelson, F. Schedin, D. C. Elias, J. A. Jaszczak, and A. K. Geim, Phys. Rev. Lett. **100**, 016602 (2008).
 - [2] X. Du, I. Skachko, A. Barker and E. Y. Andrei, Nature Nanotech. **3**, 491 (2008).
 - [3] K. I. Bolotin, K. J. Sikes, J. Hone, H. L. Stormer, and P. Kim, Phys. Rev. Lett. **101**, 096802 (2008).
 - [4] H. A. Castro Neto, F. Guinea, N. M. R. Peres, K. S. Novoselov and A. K. Geim, Rev. Mod. Phys. **81**, 109 (2009).
 - [5] M. Lewkowicz, B. Rosenstein and D. Nghiem, Phys. Rev. B **84**, 115419 (2011).
 - [6] M. I. Katsnelson, Eur. Phys. J. B **51**, 157 (2006).
 - [7] J. Tworzydło, B. Trauzettel, M. Titov, A. Rycerz, and C. W. J. Beenakker, Phys. Rev. Lett. **96**, 246802 (2006).
 - [8] M. Lewkowicz and B. Rosenstein, Phys. Rev. Lett. **102**, 106802 (2009); H. C. Kao, M. Lewkowicz, and B. Rosenstein Phys. Rev. B **82**, 035406 (2010).
 - [9] F. Schedin, A. K. Geim, S. V. Morozov, E. W. Hill, P. Blake, M. I. Katsnelson, and K. S. Novoselov, Nature Mat. **6**, 652 (2007).
 - [10] E. W. Hill, A. Vijayaraghavan, and K. Novoselov, IEEE Sensors J. **11**, 3161 (2011).
 - [11] P. Thalmeier, B. Dóra, and K. Ziegler, Phys. Rev. B **81**, 041409(R) (2010).
 - [12] V. I. Talyanskii, D. S. Novikov, B. D. Simons, and L. S. Levitov, Phys. Rev. Lett. **87**, 276802 (2001).
 - [13] C.-H. Park, L. Yang, Y.-W. Son, M. L. Cohen, and S. G. Louie, Phys. Rev. Lett. **101**, 126804 (2008).
 - [14] M. Yankowitz, J. Xue, D. Cormode, J. D. Sanchez-Yamagishi, K. Watanabe, T. Taniguchi, P. Jarillo-Herrero, P. Jacquod, and B. J. LeRoy, Nat. Phys. **8**, 382 (2012).
 - [15] L. Brey and H. A. Fertig, Phys. Rev. Lett. **103**, 046809 (2009).
 - [16] J. Dietel and H. Kleinert, Phys. Rev. B **84**, 121404(R) (2011).
 - [17] C.-H. Park, Y.-W. Son, L. Yang, M. L. Cohen, and S. G. Louie, Phys. Rev. Lett. **103**, 046808 (2009).
 - [18] P. Burset, A. L. Yeyati, L. Brey, and H. A. Fertig, Phys. Rev. B **83**, 195434 (2011).
 - [19] D. P. Arovas, L. Brey, H. A. Fertig, E. -A. Kim, and K. Ziegler, New Journal of Physics **12**, 123020 (2010).
 - [20] M. Barbier, P. Vasilopoulos, and F. M. Peeters, Phys. Rev. B **81**, 075438 (2010).
 - [21] V. Maslov and M. V. Fedoriuk, *Semi-classical approxi-*

- mation in quantum mechanics* (Reidel, Dodrecht, Netherlands).
- [22] D. J. Thouless, Phys. Rev. B **27**, 6083 (1983).
 - [23] E. Prada, P. San-Jose, and H. Schomerus, Phys. Rev. B **80**, 024414 (2009)
 - [24] C. -H. Park, Y. -W. Son, L. Yang, M. L. Cohen, and S. G. Louie, Nano Lett. **8**, 2920 (2008).
 - [25] A. V. Mamishev, K. Sundara-Rajan, F. Yang, Y. Du, M. Zahn, Proc. IEEE **92**, 808, (2004)